AD-A110 924 DEFENCE RESEARCH ESTABLISHMENT VALCARTIER (QUEBEC) F/G 20/5
A MODEL OF THE PARA-TERPHENYL DYE LASER (UN MODELE DU LASER A C--ETC(U)
NOV 81 G FOURNIER

UNCLASSIFIED DREV-R-4224/81 NL

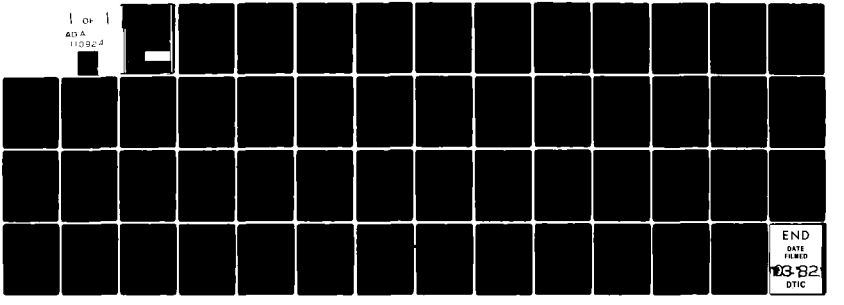

UNCLASSIFIED
UNLIMITED DISTRIBUTION

CRDA RAPPORT 4224
DOSSIER 3633-001
NOVEMBRE 1981

A MODEL OF THE PARA-TERPHENYL DYE LASER

G. Fournier

Centre de Recherches pour la Défense
Defence Research Establishment
Valcartier, Québec

BUREAU - RECHERCHE ET DEVELOPPEMENT
MINISTERE DE LA DEFENSE NATIONALE
CANADA

RESEARCH AND DEVELOPMENT BRANCH
DEPARTMENT OF NATIONAL DEFENCE
CANADA

CRDV R-4224/81
DOSSIER:3633H-007

UNCLASSIFIED

DREV R-4224/81
FILE:3633H-007

A MODEL OF THE PARA-TERPHENYL DYE LASER

by

G. Fournier

CENTRE DE RECHERCHES POUR LA DEFENSE

DEFENCE RESEARCH ESTABLISHMENT

VALCARTIER

Tel: (418) 844-4271

Québec, Canada

November/novembre 1981

NON CLASSIFIE

RESUME

Nous avons conçu un modèle théorique de laser à colorant à base de Para-Terphényl pompé par un laser excimère et nous avons établi un nouveau groupe de coefficients pour les taux de réactions du Para-Terphényl. Le problème de l'émission spontanée dans le colorant a été solutionné analytiquement. Les solutions numériques des équations du laser sont assez conformes aux résultats des expériences relatées dans la littérature.

Le modèle que nous avons élaboré nous a permis d'atteindre une efficacité et une pureté spectrale encore inconnues. (NC)

ABSTRACT

A theoretical model for a Para-Terphenyl dye laser pumped by an excimer laser has been developed. A new set of reaction-rate coefficients for Para-Terphenyl has been established. The problem of spontaneous emission in a dye has been solved analytically. The numerical solutions of the laser equations agree closely with the experimental results reported in the literature.

Use of our model resulted in the achievement of higher efficiencies and narrower linewidths than those previously reported. (U)

TABLE OF CONTENTS

1.0 INTRODUCTION

The potential of mercury-cadmium (Hg-Cd) as a blue-green excimer laser source is under evaluation at DREV for Hg-Cd is an extremely efficient emitter in the 450-550 nm wavelength which is propitious for underwater transmission. Nevertheless, to excite Hg-Cd optically, a laser emitting at 326.1 nm is required. The dye Para-Terphenyl (P-T-P) can be made to lase at this wavelength if it is pumped by an excimer laser (namely, Xe-Cl at 308 nm or Kr-F at 248 nm). We had to achieve a 10 mJ energy as well as a 10% efficiency. To reach such performances we must obtain a deep understanding of the underlying physics since previously reported efficiencies and tuning ranges for these excimer-pumped dye lasers differ considerably (Refs. 1-8).

In this report, a model of P-T-P kinetics is developed, its validity is confirmed by comparison with published experimental results and new rate constants for critical kinetic pathways are established. Preliminary results are also given for a P-T-P oscillator-amplifier system with an efficiency greater than 10% at 326.1 nm. The pumping source used is a Lumonics 262-2 Kr-F laser.

The work described herein was performed at DREV between January and September, 1980, under PCN 33H07 "Chemically Excited Lasers".

2.0 MODEL OF THE DYE KINETICS

2.1 Structure of the model

Laser action in a dye is usually controlled by a few elementary reactions. The most important ones are illustrated in Fig. 1 and described in Table I. Let us consider them rapidly. In reaction 1, dye molecules in the ground singlet state, S_0, reach the high lying ro-vibrational levels of the first electronically excited singlet state,

TABLE I

Elementary reactions controlling laser action in dyes

(1) $S_0 + h\nu_E \xrightarrow{\sigma_E} S_1$

(2) $S_1 \xrightarrow{A_f \text{ or } \sigma_f} S_1 + h\nu_f$

(3) $S_1 \xrightarrow{R_{st}} T_1$

(4) $S_1 + h\nu_E \xrightarrow{\sigma_2} S_n$

(5) $S_n \xrightarrow{R_{ics}} S_1$

(6) $T_1 + h\nu_f \xrightarrow{\sigma_{TT}} T_n$

(7) $T_n \xrightarrow{R_{ict}} T_1$

(8) $S_1 + O_2 \xrightarrow{R_{02}} T_1 + O_2$

(9) $S_1 + h\nu_f \xrightarrow{\sigma_s} S_1$

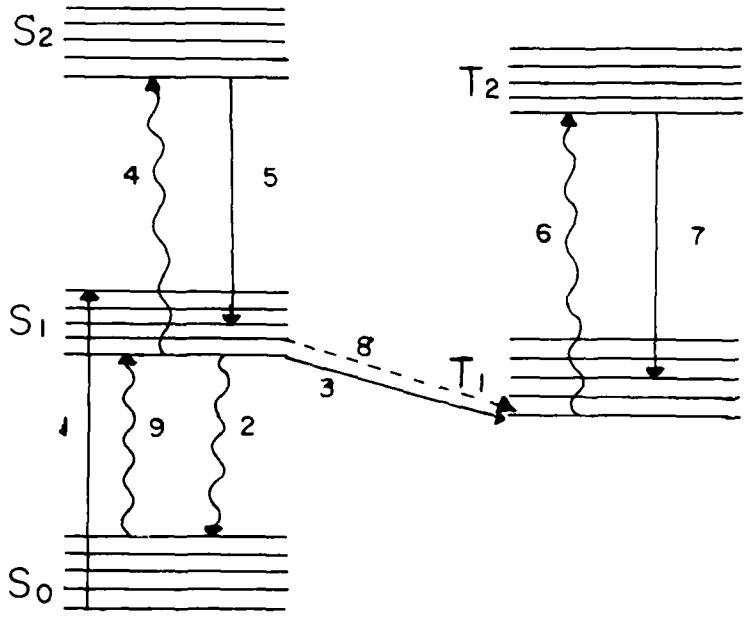

FIGURE 1 - Energy diagram of Para-Terphenyl and significant reaction mechanisms.

S_1 by absorbing photons of the appropriate wavelength. The populations within S_1 rapidly equilibrate to a Boltzmann distribution and spontaneous (A_f) and stimulated (σ_f) emission can then ensue from the lower levels of S_1 to the high lying ro-vibrational levels of S_0 (reaction 2). Rapid equilibration occurs within S_0. These two reactions account for the most pertinent processes in the laser dyes.

In reaction 3, there is a radiationless transition (R_{st}) from the first excited singlet to the first excited triplet. This transition is unfavorable to lasing because it depletes the S_1 population, producing in the triplet T_1 state molecules susceptible of absorbing a laser photon to form the triplet T_2 state (σ_{tt}) (reaction 6). This unwanted T_1 - T_n absorption, considerably affects stimulated emission at long wavelengths.

Reaction 4 also describes a loss process which occurs when the first excited singlet state, S_1, absorbs pump photons to reach higher electronic states in the singlet manifold, S_n (σ_2). The relaxation of those excited electronic states (R_{ics} & R_{ict}), called internal conversion, takes from 10^{-11}, 10^{-14}s; it is represented by reactions 5 & 7 (Ref. 9).

As they stand in air, most dye solutions become saturated with oxygen. This element being paramagnetic it tends to increase the singlet to triplet crossing rate (R_{02}). This phenomenon is summarized by reaction 8 (Ref. 9).

Reaction 9 represents the reduction of gain (σ_s) that takes place on the short wavelength side when the emission and absorption bands S_0 to S_1 overlap.

The beneficial effect of oxygen in quenching the first excited triplet state was neglected. A justification for this omission and the rejection of other unimportant processes can be found in Appendix A.

2.2 Rate Equations for Spontaneous Emission

The following set of differential rate equations, describing spontaneous emission, may be derived from the processes described in the previous section.

$$\frac{dN_s}{dt} = N_o F_o \sigma_E - N_s(A_f + R_{st} + R_{02} + F_o\sigma_2) + N_{sn} R_{ics} \qquad [1]$$

$$\frac{dN_t}{dt} = N_s(R_{st} + R_{02}) \qquad [2]$$

$$N_o + N_s + N_t + N_{sn} = N_i \qquad [3]$$

where N_o, N_s, N_t, N_{sn}, represent respectively the population densities of the S_0, S_1, T_1, S_n states; N_i is the initial population density of S_0, and F_o is the flux of photons per unit area. The first term of equation [1] is the S_0 to S_1 excitation due to the absorption of pump photons. The second one accounts for spontaneous emission. The radiationless intersystem crossing from S_1 to T_1 in the absence and presence of oxygen respectively is represented by the third and fourth terms.

The excitation caused by the pump photon absorption from the S_1 to the S_n manifold of states is expressed by the fifth term while the final term of equation [1] models the decay from the singlet manifold to the S_1 state due to internal conversion. The flux of photons, F_o, can be represented as follows:

$$F_o = I_o/h\nu_E \qquad [4]$$

where I_o is the intensity of pump radiation, and $h\nu_E$, is the photon energy at a frequency ν_E.

The first and second terms of equation [2] account for the influence of intersystem crossing on the triplet population; they are identical to terms 3 and 4 of equation [1].

Reactions 6 and 9 are unimportant here because very few photons spontaneously emitted by the dye are reabsorbed. The terms arising from those reactions have therefore been neglected in equations [1] and [2]. Equation [3] expresses the conservation of the total population density.

A further simplification arises because highly excited singlets rapidly deactivate to the S_1 state. The steady-state population may therefore be expressed as a function of N_s, and

$$N_{sn} = \frac{N_s F_o \sigma_2}{R_{ics}} \qquad [5]$$

In fact, in our system N_{sn} is less than 1% of N_s. In solving equation [1] we can therefore neglect terms five and six with little loss in accuracy. The triplet populations, T_n, may similarly be neglected.

2.3 Solution of the Rate Equations for Spontaneous Emission

Before solving, we express equations [1] and [3] in dimensionless form as follows:

$$N'_s = \frac{N_s}{N_i} \quad , \quad N'_t = \frac{N_t}{N_i} \qquad [6]$$

Substituting [6] and [3] into [1] and [2] one obtains

$$\frac{dN'_s}{dt} = (1 - N'_t) F_o \sigma_E - N'_s (F_o \sigma_E + A_f + R_{st} + R_{02}) \qquad [7]$$

$$\frac{dN'_t}{dt} = N'_s (R_{st} + R_{02}) \qquad [8]$$

Following our previous arguments we assumed a negligible population of the S_n and T_n states in deriving [7] and [8]. This system can be solved analytically as follows: we first differentiate equation [7] with respect to t and then substitute equation [8] into the resulting expression to obtain.

$$\frac{d^2N_s'}{dt^2} + \frac{dN_s'}{dt}\,(F_o\sigma_E + A_f + R_{st} + R_{02}) + N_s'\,(F_o\sigma_E)\,(R_{st} + R_{02}) = 0 \qquad [9]$$

This is an ordinary second order linear differential equation with constant coefficients. With the initial conditions $N_s' = 0$ and $N_t' = 0$, the solution is

$$N_s' = \frac{F_o\sigma_E}{(r_1 - r_2)}\,[e^{r_1 t} - e^{r_2 t}]$$

$$N_t' = \frac{F_o\sigma_E\,(R_{st} + R_{02})}{(r_1 - r_2)}\left[\frac{e^{r_1 t}}{r_1} - \frac{e^{r_2 t}}{r_2} - \left\{\frac{1}{r_1} - \frac{1}{r_2}\right\}\right]$$

$$r_1 = \frac{1}{2}\left[-(F_o\sigma_E + A_f + R_{st} + R_{02}) + \sqrt{(F_o\sigma_E + A_f + R_{st} + R_{02})^2 - 4F_o\sigma_E\,(R_{st} + R_{02})}\right]$$

$$r_2 = \frac{1}{2}\left[-(F_o\sigma_E + A_f + R_{st} + R_{02}) - \sqrt{(F_o\sigma_E + A_f + R_{st} + R_{02})^2 - 4F_o\sigma_E\,(R_{st} + R_{02})}\right] \qquad [10]$$

Equation [10] is a complete analytic description of the behavior of spontaneous emission in the presence of a pump source of constant intensity. With a time-varying pump source the behavior can be modelled to any desired degree of accuracy if the pump source is represented as piecewise constant in time and if the required boundary conditions from one time segment to the next are matched.

The energy emitted and absorbed by the dye determines the efficiency of fluorescence. The total energy (E) emitted in fluorescence per unit excited volume is given by

$$E = N_i \int_0^{t_p} N'_s A_f \overline{h\nu_f}\, dt \qquad [11]$$

where $\overline{h\nu_f}$ is the average energy of the emitted photon, and t_p is the elapsed time since the start of the pump pulse. In non-dimensional form, from [10] and [11], we have

$$\varepsilon = \frac{E}{N_i} = (A_f \overline{h\nu_f}) \frac{F_o \sigma_E}{(r_1 - r_2)} \left[\frac{e^{r_1 t_p}}{r_1} - \frac{e^{r_1 t_p}}{r_2} - \left(\frac{1}{r_1} - \frac{1}{r_2} \right) \right] \qquad [12]$$

The energy dissipated by the pumping radiation source, (S), is expressed in non-dimensional form by the following expression

$$s = \frac{S}{N_i} = \overline{h\nu_E} \int_0^{t_p} [(1-N'_t) F_o \sigma_E - N'_s F_o \sigma_E + N'_s F_o \sigma_2] dt \qquad [13]$$

The last term of [13] represents the absorption of pump photons by a transition from S_1 to S_n (reaction 4). We neglected it when evaluating the populations of the various states but we have to consider it in the energy balance because the absorption from S_1 to S_n and the subsequent rapid collisional return to S_1 is a net loss of pump energy even though there is no net change in S_1 concentration. Substitution for N'_s and N'_t from equation [10] into equation [13] yields:

$$s = F_o \overline{h\nu_E} \left[\sigma_E t_p + \frac{F_o \sigma_E (\sigma_2 - \sigma_E)}{(r_1 - r_2)} \left(\left(\frac{e^{r_1 t_p}}{r_1} - \frac{e^{r_2 t_p}}{r_2} \right) - \left(\frac{1}{r_1} - \frac{1}{r_2} \right) \right) \right.$$

$$\left. - \frac{F_o \sigma_E^2 (R_{st} + R_{02})}{(r_1 - r_2)} \left(\frac{e^{r_1 t_p}}{r_1^2} - \frac{e^{r_2 t_p}}{r_1^2} - \left(\frac{1}{r_1^2} - \frac{1}{r_1^2} \right) - \left(\frac{t_p}{r_1} - \frac{t_p}{r_2} \right) \right) \right] \qquad [14]$$

By definition, the efficiency of production of spontaneous emission, W_F, is

$$W_F = \frac{E}{S} = \frac{\epsilon}{s} \qquad [15]$$

2.4 Geometry of Side Pumping

Figure 2 is a schematic of a type of dye laser known as the 'side-pumped system' in which the radiation from the pump laser (in our case Xe-Cl or Kr-F) is focused into a line on the side of the dye cell. As this radiation penetrates into the dye it is progressively absorbed. Stimulated emission of the dye occurs between mirrors R1 and R2. This emission is transverse to the direction of the pump laser beam.

We now describe how spontaneous and stimulated emission is taken into account in the arrangement shown in Fig. 2. Equations [12] and [14] refer to the local efficiency rather than the overall spontaneous emission efficiency of a device such as the one shown in Fig. 2. From equations [12] to [15], we see that the local efficiency of fluorescence at a given point is a function of the photon flux at that point.

Because of the occurrence of an excited state absorption from S_1 to S_n, the absorption of pump radiation does not follow Beer's law. For the same reason, the efficiency of fluorescence increases as the flux of pump photons diminishes within the dye solution. Therefore equation [14] must be integrated over the entire penetration depth of the pump radiation.

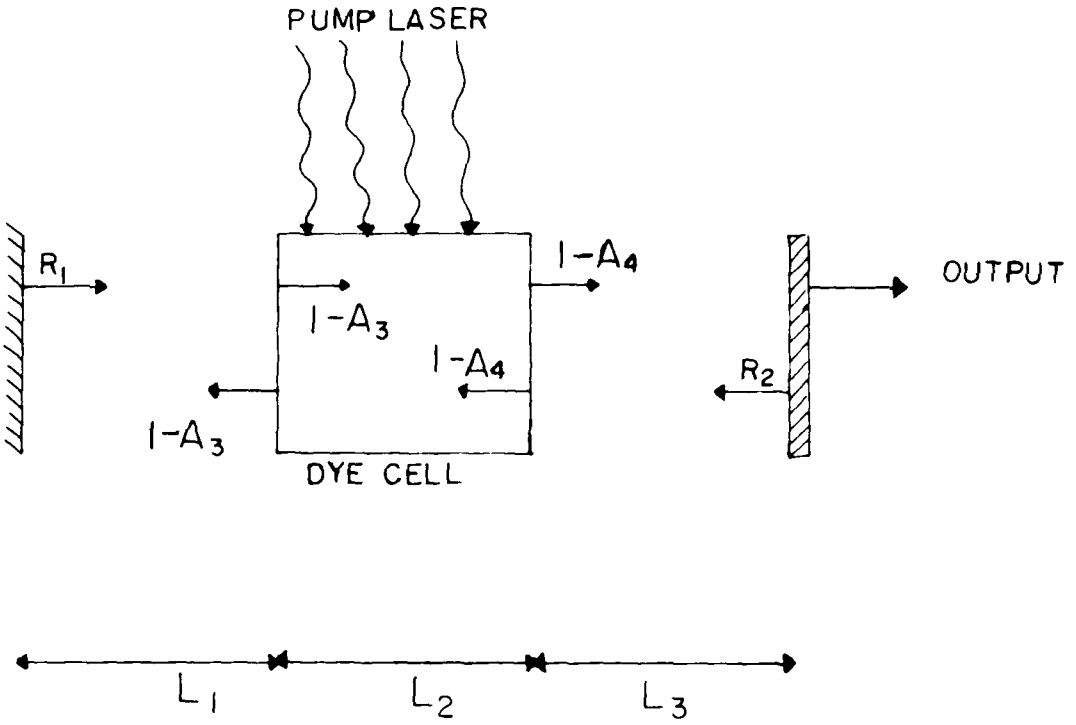

FIGURE 2 - Dye laser, side pumping geometry

The flux of pump photons incident on the entrance face of the dye cell is constant in time. However, at any finite depth within the dye, the flux will vary in time. A first order estimate of the energy lost during the pump pulse, at a given depth in the dye, can be made from eqs. [13] and [14]. The flux of photons can be reduced by an appropriate time-averaged quantity and eqs. [12] and [14] can be recomputed for this new average flux. This procedure is expressed by the following formula:

$$F_o(x) = F_o(o) - \frac{1}{t_p \overline{h\nu_E}} \int_o^x s(F_o(x))\, N_i dx \qquad [16]$$

where t_p is the pulse length and x is the distance from the entrance face of the dye cell.

We can renormalize [16] as follows by defining

$$dU = N_i dx \qquad [17]$$

$$F_o(U) = F_o(o) - \frac{1}{t_p \overline{h\nu}_E} \int_o^U s(F_o(U))dU \qquad [18]$$

Therefore, a device as the one shown in Fig. 2 has an overall efficiency for spontaneous emission that can be expressed as:

$$W_F = \frac{\int_o^U \varepsilon(F_o(U))dU}{\int_o^U s(F_o(U))dU} \qquad [19]$$

Equations [18] and [19] approximately account for the finite penetration of radiation in the dye. Since we considered the effects of the pumping geometry on the efficiency of spontaneous emission, we could directly compare this efficiency with that of stimulated emission in a similar geometry.

3.0 NEW RATES COEFFICIENTS FOR PARA-TERPHENYL

To use our model, we require rate coefficients for the processes listed in Table I. As mentioned before, those reported in the literature on Para-Terphenyl are discrepant. Only by inferring new values for the rate coefficients were we able to resolve those discrepancies and obtain a consistent picture. The new set of coefficients established through our analysis is studied hereafter.

3.1 Spontaneous and Stimulated Emission Coefficients

The quantum yield of fluorescence for a dye is defined as the ratio of the number of photons emitted by the dye in the fluorescence band to the number of photons absorbed by the $S_0 \rightarrow S_1$ transition. For a given dye the results obtained are frequently reported with respect to a standard dye solution.

In Reference 10, the quantum yield of fluorescence, Q_F, is given as 0.93 for a deoxygenated solution of Para-Terphenyl. A witness solution of 9,10-diphenylanthracene was arbitrarily assigned a quantum yield of one. Recent papers demonstrate that the absolute quantum yield of thi. reference solution is 0.95 (Refs. 11-12). We can therefore say that the quantum yield for a deoxygenated solution of P-T-P is

$$Q_F^D = 0.93 \times 0.95 = 0.88 \qquad [20]$$

The ratio of quantum yields of a deoxygenated to an oxygen-saturated solution of Para-Terphenyl is 1.07 (Ref. 10). The oxygen-saturated quantum yield is thus:

$$Q_F^S = 0.88/1.07 = 0.82 \qquad [21]$$

Reference 13 states that the intersystem crossing quantum yield in a deoxigenated solution of Para-Terphenyl is 0.12. In such a solution, the sum of the fluorescence (0.88) and the intersystem crossing (0.12) quantum yields is thus equal to 1.0 and apparently, the other loss processes are unimportant.

Oxygen greatly influences the rate of intersystem crossing. Assuming that the difference in quantum yields is due to intersystem crossing (reaction 3) we have

$$Q_F^D = \frac{A_f}{A_f + R_{st}} \qquad [22]$$

where A_f is the Einstein coefficient of spontaneous emission (reaction 2) and R_{st} is the pseudo-first order rate coefficient for intersystem crossing (reaction 3). In the absence of O_2, the fluorescence decay time, t_s has been measured as 0.95 ns (Ref. 10).

Since

$$\frac{1}{t_s} = A_f + R_{st} \qquad [23]$$

it follows that

$$A_f = \frac{Q_F^D}{t_s} = \frac{0.88}{0.95 \times 10^{-9}} = 9.3 \times 10^8 \ s^{-1} \qquad [24]$$

The natural decay time of Para-Terphenyl is therefore 1.08 ns.

With the spontaneous decay coefficient, A_f, and the fluorescence line shape (Ref. 10), it is possible to estimate the stimulated emission cross section (reaction 2) using the following formula

$$\sigma_f(\nu) = \frac{A_f}{8\pi} \frac{\lambda^2}{n^2} L(\nu) \qquad [25]$$

In the above equation, $L(\nu)$ is the normalized line shape factor, λ the wavelength, ν the frequency of emission, and n the index of refraction of the dye solution. The stimulated emission cross section thus calculated as a function of the wavelength is given in Fig. 3.

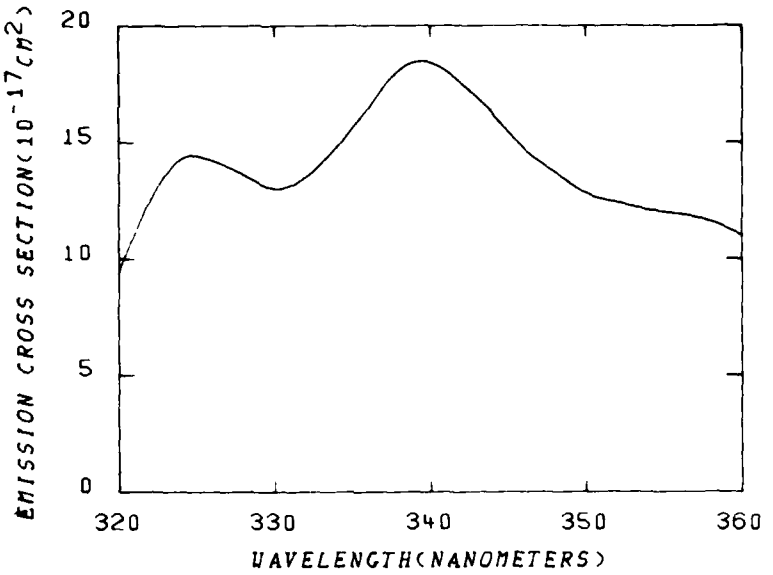

FIGURE 3 - Stimulated emission cross section of the S_1 state of Para-Terphenyl

3.2 Intersystem Crossing Rate

Equation [22] can be rewritten as

$$R_{st} = \frac{A_f}{Q_F^D} - A_f \qquad [26]$$

Given the values of A_f and Q_F^D established above, we have for reaction 3

$$R_{st} = 1.27 \times 10^8 \ s^{-1} \qquad [27]$$

The intersystem crossing time is therefore 7.9 ns.

In the case of an oxygen-saturated solution, we must include the effect of oxygen on the intersystem crossing rate (reaction 8). We write

$$Q_F^S = \frac{A_f}{(A_f + R_{st} + R_{02})} \qquad [28]$$

Therefore

$$R_{02} = \frac{A_f}{Q_F^S} - (A_f + R_{st}) \qquad [29]$$

Evaluating the terms on the right hand side of [29] we find

$$R_{02} = 0.77 \times 10^8 \ s^{-1} \qquad [30]$$

The oxygenated triplet crossing time is therefore 4.9 ns.

3.3 Ground-State Absorption

The cross section of the Para-Terphenyl ground-state absorption is given in Ref. 10 and shown in Fig. 4. This cross section accounts for reaction 1. It was pointed out previously that the same ground-state absorption can contribute significantly to a gain reduction on the short wavelength side of the fluorescence band.

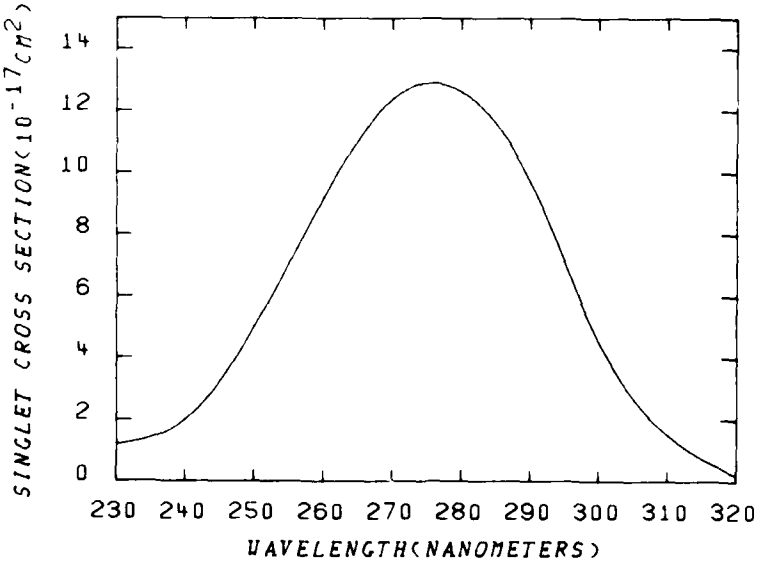

FIGURE 4 - S_0 to S_1 absorption cross section of Para-Terphenyl

The center wavelength of emission of Para-Terphenyl is 340 nm. An expanded scale of the S_0 - S_1 absorption in this wavelength region is given in Fig. 5 (reaction 9).

As mentioned before (Section 2.2) internal conversion (reactions 5 & 7) is known to be fast. Because of this rapid equilibration within the singlet manifold we neglect processes (4) and (7).

3.4 Excited Singlet Absorption

Tomin et al. (Ref. 3) have measured the behavior of fluorescence when a P-T-P solution is pumped by a Kr-F laser of varying intensity. They found that the efficiency of fluorescence decreases when the power density of the pump beam increases. This phenomenon indicates the presence of S_1 to S_n transitions; it is expressed by reaction (4) which is included in the estimate of the efficiency of spontaneous emission.

Given the model developed in section 2 and the rates coefficients estimated above, it is possible to estimate the S_1 to S_n transition cross section by iterative fitting. As shown in Fig. 6, the best estimate obtained was 2.5×10^{-18} cm^2. To demonstrate the sensitivity of the results, a fit with a cross section of 1.0×10^{-17} cm^2 was plotted; the results appear as a dashed line in Fig. 6.

3.5 Excited Triplet Absorption

It is known that different solvents, can shift the wavelength of Triplet-Triplet absorption by 20 nm or more. Since P-T-P fluorescence is on the short wavelength side of T_1 to T_n absorption (reaction 6) such a shift would have a drastic effect on the gain of the laser. For P-T-P in solution, the T_1 to T_n absorption cross section has been measured with n-hexane as a solvent (Refs. 13, 14, 15), but no experimental data was available for cyclohexane. We thus

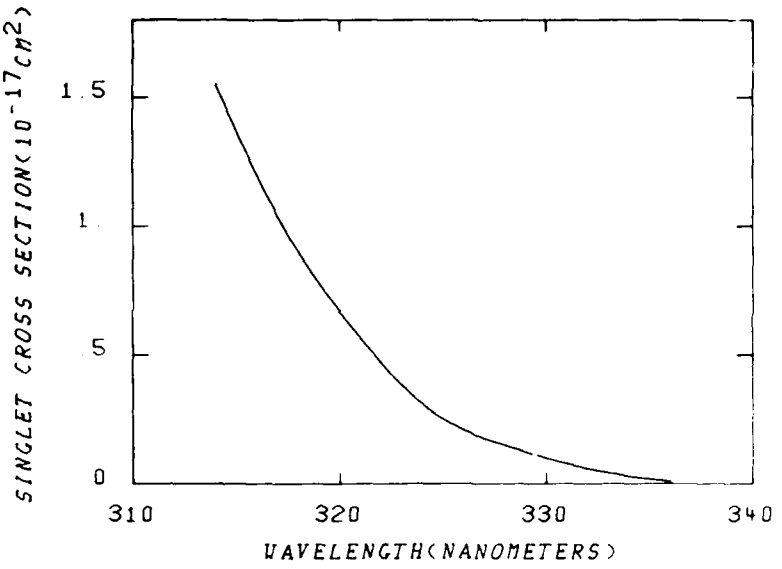

FIGURE 5 - Expanded view of the long wavelength portion of the S_0 to S_1 absorption cross section of Para-Terphenyl

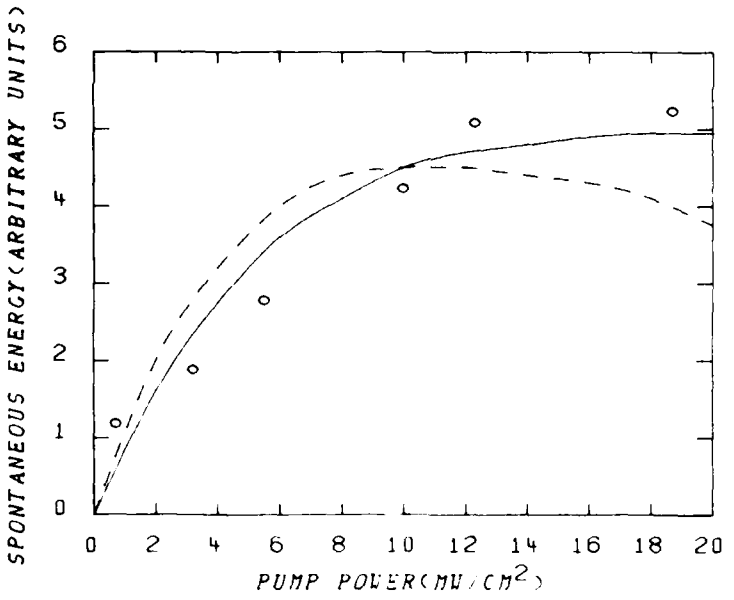

FIGURE 6 - P-T-P spontaneous emission energy as a function of Kr-F pump power.

pump power.

o experimental points (3)

——— Theory σ_2 = 2.5 x 10^{-18} cm^2.

------ Theory σ_2 = 1 x 10^{-17} cm^2.

utilized the line shape observed with n-hexane after having adjusted the absolute values of the cross section by fitting the results of our model of laser action to one set of experimental points (Ref. 1). The resulting cross section is shown in Fig. 7.

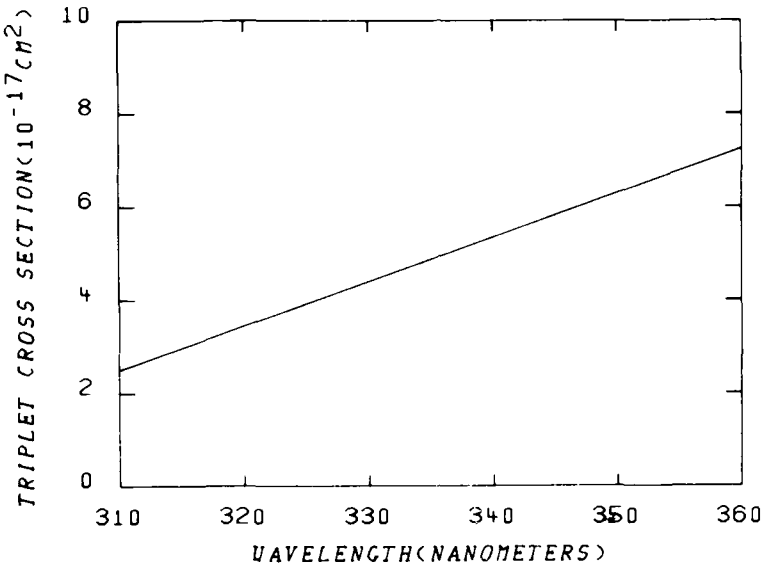

FIGURE 7 - T_1 to T_n triplet-triplet absorption cross section

One should note that since the line shape is given by a straight line in the wavelength region of interest, our procedure of using the same slope but adjusting the amplitude is equivalent to assuming a wavelength shift in T_1 to T_n absorption.

With this estimate of the extent of T_1 to T_n absorption (reaction 6) we now have in hand all required kinetic rates to describe laser action in P-T-P.

4.0 LASER CAVITY MODEL

The geometry of the laser model can best be understood by reference to Figs. 2 and 8. By a cylindrical lens (not shown), a beam of photons from a Kr-F or Xe-Cl laser is focused into a thin stripe on the side of a dye cavity. This beam penetrates to an average depth, δ, into the cell; it covers the entire length, L2, of the cell and its height is H. Laser action in the dye will occur in a direction normal to the mirror (or grating) R1 and to the partially transmitting mirror R2. R1 and R2 also denote the value of the reflectivity of these optical elements. A3 and A4 denote the loss suffered by the beam at the entrance and exit faces of the dye cell. Any additional loss at mirrors R1 and R2 will be denoted by A1 and A2, the fractional power loss of these elements. L1 is the distance between the mirror (or grating) R1 and the dye cell. L2 is the distance between the dye cell and the output coupler R2. The total distance between mirrors is given as

$$L = L1 + L2 + L3 \qquad [31]$$

In a laser-pumped dye-laser system, the gain is large. Once above threshold, the laser thus reaches saturation very early in the pulse. The rate of growth or decay of the laser from then on depends only on the pump pulse and the kinetics of the dye. The total light flux (i.e. two ways) in a cavity operating at saturation cannot differ significantly from point to point along the laser axis. Consequently, spatial gradients in the flux along the laser axis are negligible when compared with the rate of growth or decay of this flux. The equations which describe the flux of photons in the cavity can therefore legitimately be averaged along the lasing axis. Little accuracy is lost by that procedure and the equations are greatly simplified.

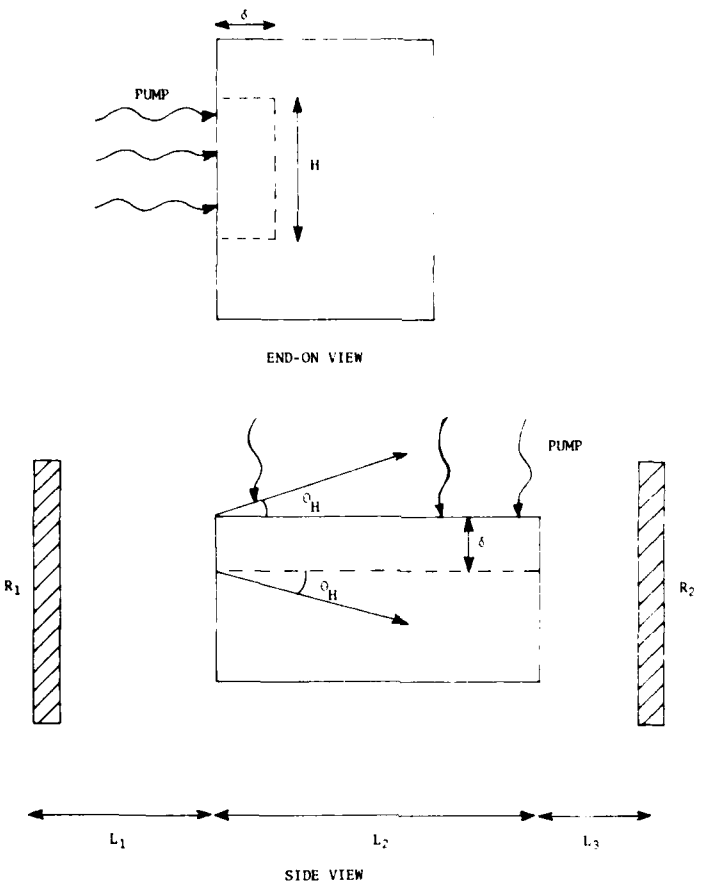

FIGURE 8 - Schematic of diffraction effects

However, this spatial average cannot be carried out in the direction perpendicular to the laser axis, i.e. along the pump beam which loses its energy in penetrating the dye. The pump photon flux at any given depth in the dye differs significantly from the flux impinging on the dye cell face. The effect we described for spontaneous emission in Section 2.4 is operative here.

We must therefore solve the longitudinally averaged laser equations at every depth until a distance of penetration is reached where the pump laser flux becomes negligible. The results must then be integrated along the axis parallel to the pump beam.

4.1 Local Laser Equations

At any given depth of penetration in the dye, laser action can thus be modelled by the following equations:

$$\frac{dN'_s}{dt} = (1-N'_t)(F_o\sigma_E + \omega'\sigma_s) - N'_s(F_o\sigma'_E + A_f + R_{st} + R_{2,} + c'(\sigma_f + \sigma_s)) \qquad [32]$$

$$\frac{dN'_t}{dt} = N'_s\,(R_{st} + R_{2,}) \qquad [33]$$

$$\frac{d\omega'}{dt} = c' N_i C\left\{\left[N'_s\,(\sigma_f + \sigma_s - \sigma_2) - N'_t\,(\sigma_{TT} - \sigma_s) - \sigma_s\right]\frac{L2}{L}\right.$$

$$- \frac{1}{N_i L}\left[\frac{A1}{2} + \frac{A2}{2} + A3 + A4 + \frac{(1-A1-R1)}{2} + \frac{(1-A2-R2)}{2}\right.$$

$$\left.\left. + \lambda(L1 + L3 + \frac{L2}{n})\left(\frac{1}{\quad} + \frac{1}{H}\right)\right]\right\} + N_i C N'_s\, A_f\left(\frac{\sigma_f(\lambda)}{\sigma_f(MAX)}\right)\left(\frac{d\lambda}{\Delta\lambda}\right)\left(\frac{\lambda^2}{H}\right)\frac{1}{2(\quad)} \frac{L2}{L} \qquad [34]$$

$$\omega' = \frac{\omega}{h\nu_f} \quad , \quad \omega_{out} = \frac{\omega}{2}(1-A2-R2) \qquad [35]$$

where C is the speed of light, n is the index of refraction of the dye solution, ω is the two way light flux inside the cavity in watts/cm^2 and ω_{out} is the output power of the laser. Equation [32] is the same equation we encountered when dealing with spontaneous emission [1] except for the two terms involving ω' which describe stimulated emission from S_1 to S_0 and absorption into S_1 from S_0.

Equation [33] is identical to the one describing spontaneous emission [2]. A term to account for triplet-triplet absorption of laser radiation could have been included but, as we mentioned before for spontaneous emission, internal conversion dominates; the effect of this term on the kinetics would thus be negligible.

Equation [34] describes the buildup of laser radiation inside the cavity. The first term in square brackets represents the gain in the cavity. In this case some terms account for S_1 to S_n and T_1 to T_n absorption. Because of the enormous reverse rate of internal conversion, they do not influence the population of the singlet and triplet states but they do absorb some laser radiation. This is similar to the case of spontaneous emission where σ_2 had to be accounted for in the energy balance equation but not in the kinetic equations.

The second term of [34] represents losses due to optical components and to diffraction. A more detailed description of this last term will be given in Section 4.2.

The last term of this equation is usually referred to as the noise or source term. It is inserted to account for spontaneous emission in the bandwidth, $d\lambda$, and solid angle, $d\Omega$, of laser emission. In this case, the spontaneous emission is assumed to be gaussian, with a 1/e full width of $\Delta\lambda$. $\sigma_f(MAX)$ is the cross section for stimulated emission at the band center and $\sigma_f(\lambda)$ is the cross section at the laser wavelength λ.

It is further assumed that

$$d\Omega = \frac{\lambda^2}{\delta H} \frac{1}{4\pi} \qquad [36]$$

which is the diffraction limited solid angle of emission of the laser. The section that follows discusses the effects of diffraction.

Equations [32]-[35] were numerically integrated using a standard implicit finite difference scheme.

4.2 Diffraction Effects in the Cavity

We treat the cross-sectional area of excited dye as if it were a diffracting aperture. The high gain present in this region strongly amplifies the portion of the wavefront passing through it while the wavefront outside this region remains relatively unaffected. The resulting amplitude difference between these two zones produces a diffraction pattern similar to that given by a rectangular aperture of height H and width · (Fig. 8). The exact near-field pattern in a high-gain medium is difficult to model, but a first-order approximation can be made if one remembers that the far field pattern of a rectangular aperture has a first minimum occurring at an angle

$$ = \lambda/2an \qquad [37]$$

where a is the relevant lateral dimension of the aperture, n is the index of refraction of the medium, and λ is the free-space wavelength. The horizontal and vertical diffraction half angles are

$$\theta_H = \frac{\lambda}{2Wn} \quad , \quad \theta_V = \frac{\lambda}{2Hn} \qquad [38]$$

For small diffraction angles the total solid angle subtended by the principal lobe of radiation of the laser is therefore given by

$$d\Omega = \frac{\lambda^2}{\delta H} \frac{1}{4\pi} \qquad [36]$$

as was mentioned in the previous section. Here, diffraction manifests itself as if there were a lateral flux of photons out of the excited dye volume resulting in an unwanted loss.

In Figure 8, we see that the dye laser flux entering the excited dye volume is given by

$$\text{Flux} = \omega H \delta \qquad [39]$$

and the component of the flux perpendicular to the laser axis in the direction of the side walls by

$$\omega \sin\theta_H \approx \frac{\omega\lambda}{2\delta n} \qquad [40]$$

The components of the flux going through the top and bottom surfaces are expressed by

$$\omega \sin\theta_V \approx \frac{\omega\lambda}{2Hn} \qquad [41]$$

Integrating these fluxes over the top, bottom, and side surfaces over the whole length of the dye laser, for the total lost flux, we obtain I_d,

$$I_d = \omega\lambda\left[L1\left(\frac{H}{\delta} + \frac{\delta}{H}\right) + \frac{L2}{n}\left(\frac{H}{\delta} + \frac{\delta}{H}\right) + L3\left(\frac{H}{\delta} + \frac{\delta}{H}\right)\right] \qquad [42]$$

The fraction of the flux lost through diffraction is the ratio of [42] and [39]; it gives

$$f = \lambda\left(L1 + \frac{L2}{n} + L3\right)\left(\frac{1}{\delta^2} + \frac{1}{H^2}\right) \qquad [43]$$

This is also the last term in the second square brackets of equation [34]. It accounts for the losses out of the excited dye volume due to diffraction effects. Those effects are responsible for the discrepancies found in the literature on the efficiency of Para-Terphenyl lasers. The magnitude of those effects depends critically on the laser geometry.

5.0 COMPARISON WITH EXPERIMENTS

Table II lists the various experiments we modelled. The values of the relevant parameters used in our model of each experiment are also given in this table. In all cases we used a constant pump laser intensity as a function of time. The pulse length matched the reported width at half maximum of the pump pulse. The cross section for triplet-triplet absorption was obtained by fitting the untuned laser results of Zapka (Ref. 1); it was used in all cases.

TABLE II

Experiment	L1 cm	L2 cm	L3 cm	A1	A2	A3	A4	R1	R2	R cm	Io (MW/cm²)	Tp (ns)	Concentration (M/L)
Ref. [1] Fig. 9	1.	2.	1.	.05	.04	.04	.04	.95	.04	.1	2.0 to 10.	14	1.1×10^{-3}
Ref. [1] Fig. 10	2.5	2.	2.5	.7	.001	.04	.04	.3	.2	.1	2.0	14	1.1×10^{-3}
Ref. [5] Fig. 11	.15	2.	.15	.3	.001	.001	.001	.7	.04	.1	.2 to 1.	5.	1.0×10^{-3}
Ref. [3] Fig. 12 & 13	.6	1.8	.6	.05	.001	.04	.04	.95	.08	.15	2. to 20.	40.	1.25×10^{-3}
Ref. [6] Fig. 14	5.7	.6	5.7	.05	.04	.04	.04	.95	.04	.2	6. to 60.	20.	1.3×10^{-3}
Ref. [6] Fig. 15	5.0 to 25.0	.6	5.0 to 25.0	.05	.04	.04	.04	.95	.04	.2	50.	20.	2.5×10^{-3}
Ref. [6] Fig. 16	5.7	.6	5.7	.05	.04	.04	.04	.95	.04	.2	50.	20.	5×10^{-4} 2.5×10^{-3}
Ref. [8] Fig. 17	1.6	.8	1.6	.05	.001	.04	.04	.95	.08	.2	.1 to 10.	34.	2×10^{-3}
Ref. [7] Fig. 18	2.	1.	2.	.7	.001	.00	.00	.3	.7	.1	50.	12.	1×10^{-3}

Different solvents have different spectral shifts of the triplet-triplet absorption band. Our procedure presently neglects this factor. Strictly, the results should be considered valid only when cyclohexane is employed as a solvent. However, the comparison was also carried out for other solvents (Refs. 3 & 6) and no significant discrepancies were found between experiment and theory.

5.1 Krypton-Fluoride Pump Laser

The first experiment modelled was that of Zapka et al (Ref. 1). As mentioned previously, their results were used to obtain a value of the triplet-triplet absorption cross section for Para-Terphenyl with cyclohexane as a solvent. As shown in Fig. 9, the linear dependence of output energy on input energy means that efficiency is independent of pump intensity. This differs from the behavior observed for spontaneous emission (Fig. 6) and requires an explanation. The loss of efficiency of spontaneous emission with pump power is due to $S_1 \rightarrow S_n$ absorption. In a laser cavity operating at saturation, this effect is minimized because, owing to stimulated emission, the population of the S_1 state and its resultant absorption are reduced. Pump photons excite the S_1 state but laser photons deplete it as quickly. For the same reason, the ground state S_0 population is also maintained at a much higher level in a laser than in the case of spontaneous emission. Because of this higher ground state population the absorption depth is quite different from what it is in the case of emission. When lasing occurs, the absorption depth tends to be much shorter. In fact, except for very high concentrations ($> 2 \times 10^{-3}$ Molar), it is quite close to that calculated from Beer's law. The "burn-through" or bleaching effect is considerably reduced and lasing occurs closer to the entrance of the dye cell than would be expected by monitoring spontaneous emission.

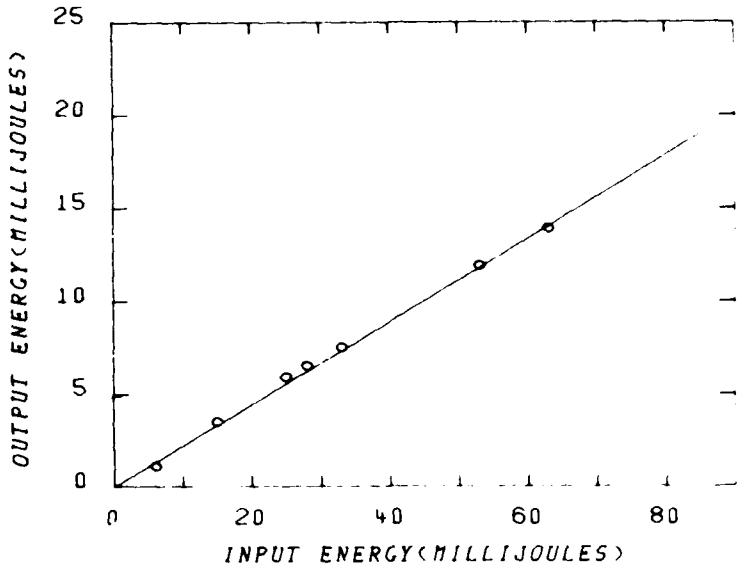

FIGURE 9 - P-T-P output energy against Kr-F pump energy.
o experimentals points (Ref. 1).
—— for theory

Figure 10 shows the results of a second experiment by Zapka (Ref. 1) where Para-Terphenyl was tuned by replacing the total reflector in the cavity by a holographic grating. Since the pump beam height was not specified, we used an estimate of 1 mm. The solid line in Fig. 10 represents our results. The overall goodness of the fit in this particularly sensitive case gives substantial confidence in the accuracy of our model.

Our model was also compared to an experiment carried out by Godard and de Witte (Ref. 5); the results are shown in Fig. 11. Those authors used a very short low-energy laser pulse. Their results and ours are in good agreement for a molar concentration of 1×10^{-5}. However, they are significantly discrepant at a molar concentration of 5×10^{-5} because we used Beer's law to estimate the absorption depth, δ, in our diffraction loss term. As the concentration is increased, δ becomes very small. At such high concentrations a

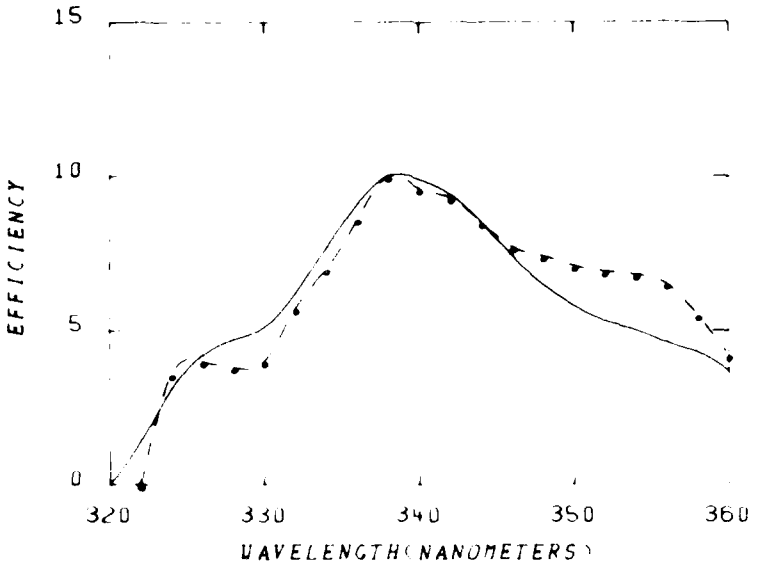

FIGURE 10 - Efficiency as a function of wavelength for Kr-F-pumped P-I-P.
---o--- experimental points from ZAPKA et al. (Ref. 1)
——— for theory

FIGURE 11 - Kr-F-pumped P-I-P. Experimental results taken from Godard and de Witte (Ref. 5).
----- experiment, molar concentration 5×10^{-3}
-.-.- experiment, molar concentration 1×10^{-3}
——— molar concentration theory, 5×10^{-3}
..... molar concentration theory, 1×10^{-3}

certain amount of bleaching by the pump laser beam does occur even with lasing. The effective depth therefore becomes larger than the one calculated. This dynamic effect could be modelled but at the expense of some further complexity in the model.

The temporal behavior of the Para-Terphenyl dye laser is compared with an experiment by Tomin et al. (Ref. 3) in Figs. 12 and 13. Only the decay time is illustrated; the experimental results are shown as a broken line and the theory as a solid one. The pump pulse lengths were taken directly from oscilloscope traces given in Ref. 3. Figure 12 refers to a near threshold pump pulse energy of 10 mJ and Fig. 13 to a pump pulse energy ten times greater. In both cases the fit is good. The similarity of the decay times indicates that the mechanisms controlling the length of the pulse are triplet-triplet absorption and singlet to triplet transition time. Their effect is almost independent of pump pulse intensity.

McKee and James (Ref. 6) carried out experiments using a Lumonics 262 excimer laser with a laser pulse length of 20 ns in Kr-F and P-dioxane as a solvent. In our model, we assumed the same triplet-triplet cross section as the one used in Zapka's experiment (Ref. 1). The fit obtained for an untuned oscillator is shown in Fig. 14. It is particularly interesting to note that the estimate of the threshold energy seems to match our theoretical prediction quite well.

McKee and James (Ref. 6) also carried out a set of experiments where they varied the length of their laser cavity and observed the resulting relative output. This experiment is a sensitive test of the accuracy of the diffraction loss term as this term is the one most affected by a change of the resonator length. Figure 15 shows that our theory predicts a somewhat sharper falloff with distance than the one actually observed. This discrepancy means that we somewhat overestimated this loss term, possibly because the excited dye cross

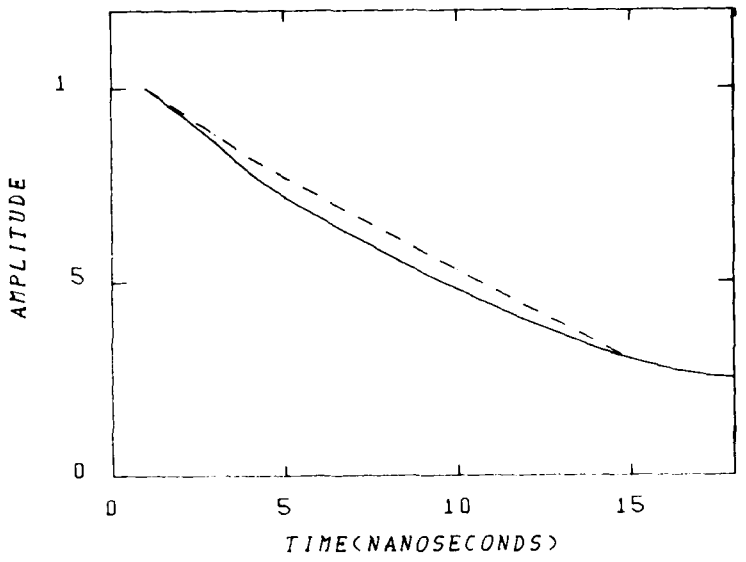

FIGURE 12 - P-T-P laser pulse decay time
----- experiment, 10 mJ Kr-F pump energy (Ref. 3)
——— theory

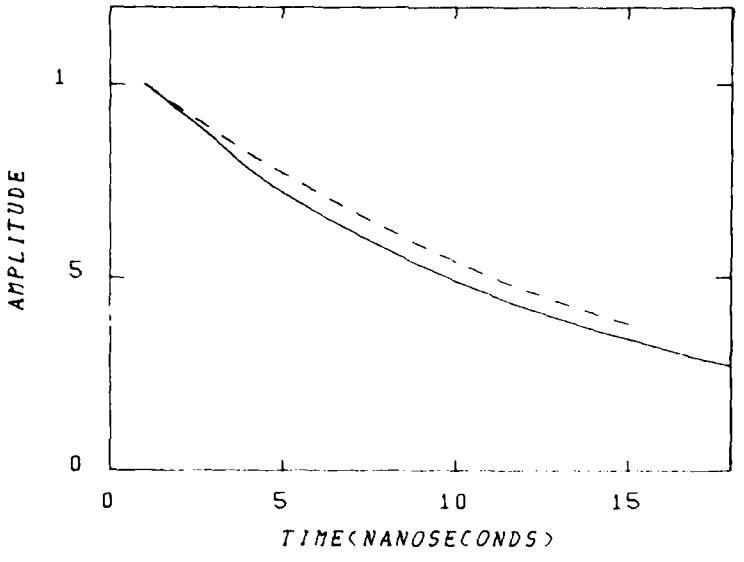

FIGURE 13 - P-T-P laser pulse decay time
----- experiment, 100 mJ Kr-F pump energy (Ref. 3)
——— theory

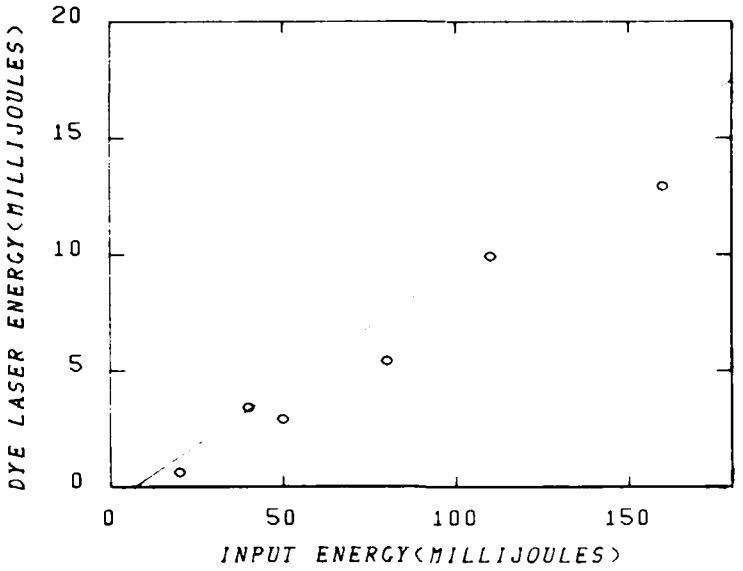

FIGURE 14 - P-T-P laser energy as a function of Kr-F pump energy
o McKee and James' experiment (Ref. 6)
—— · theory

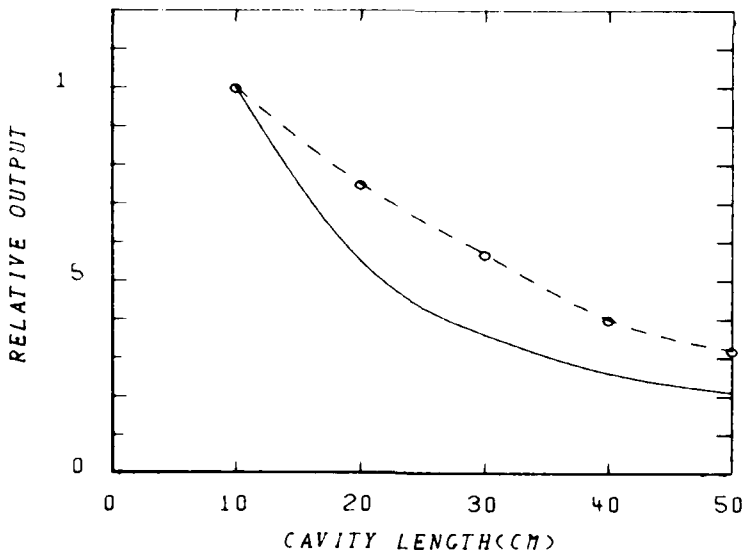

FIGURE 15 - P-T-P relative laser output as a function of cavity length at a molar concentration of 2.5×10^{-3}
--o--o-- McKee and James' experiment (Ref. 6)
———— theory

section is not as sharp edged as we assumed. The effective aperture would be better represented as a smoothly varying function of the penetration depth giving rise to a form of apodization, and thus reducing the loss.

Figure 16 shows a comparison of experiment (Ref. 6) and theory for the output power of Para-Terphenyl as a function of concentration. Neglecting the effect of bleaching on the diffraction loss results in an underestimate in the high concentration range.

The exact cause of the divergence between theory and experiment in the low concentration range is not clear at this time.

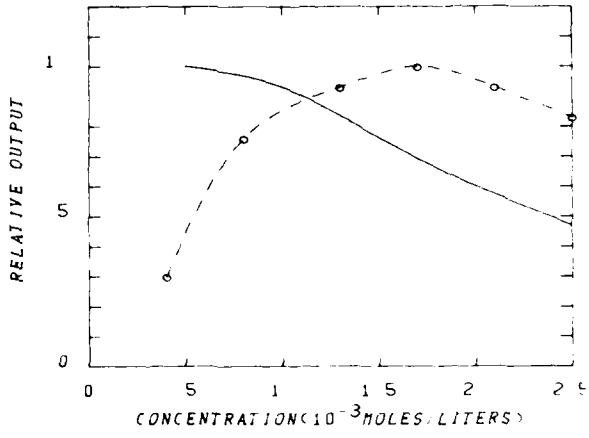

FIGURE 16 - P-T-P relative laser output as a function of concentration for a 12-cm cavity length
--o--o-- McKee and James' experiment (Ref. 6)
———— theory

5.2 Xenon-Chloride Pump Laser

Modelling Xe-Cl (308 nm) as a pump source for a Para-Terphenyl laser gives rise to several new difficulties. For instance, no data is available for the efficiency of spontaneous emission as a function of pump laser intensity. Therefore, the S_1 to S_n absorption cross

section cannot be estimated. In a laser operating far above threshold this reaction will not be as significant because stimulated emission keeps the population of S_1 small.

For our purposes we used the value of S_1 to S_n absorption derived from the Kr-F results and we applied it to Xe-Cl. The cross section of the other reactions given in Section 3 were appropriately corrected for a 308 nm pumping radiation.

Figure 17 shows the comparison between theory and experiment for an untuned laser pumped by a 34-ns Xe-Cl pulse (Ref. 8). The theory errs somewhat on the conservative side. The threshold behavior seems to be rather well accounted for. This would indicate that the S_1 to S_n absorption of Xe-Cl at 308 nm and Kr-F at 249 nm does not differ greatly.

Figure 18 compares theory and experiment for a tunable laser built by Hollins and Webb (Ref. 7). In this case, the theory overestimates the magnitude in the wings of the transition and underestimates the peak value. Problems with cavity alignment as one tunes the laser could partially account for this discrepancy. Those problems would be much more significant in the wings of the transition, i.e. near threshold. The grating used in this case was operated in 7th order and it is very difficult to estimate the efficiency as a function of wavelength of such a grating operating in a high order. We thus used a constant value independant of wavelength. This could account for some of the observed differences between experiment and theory.

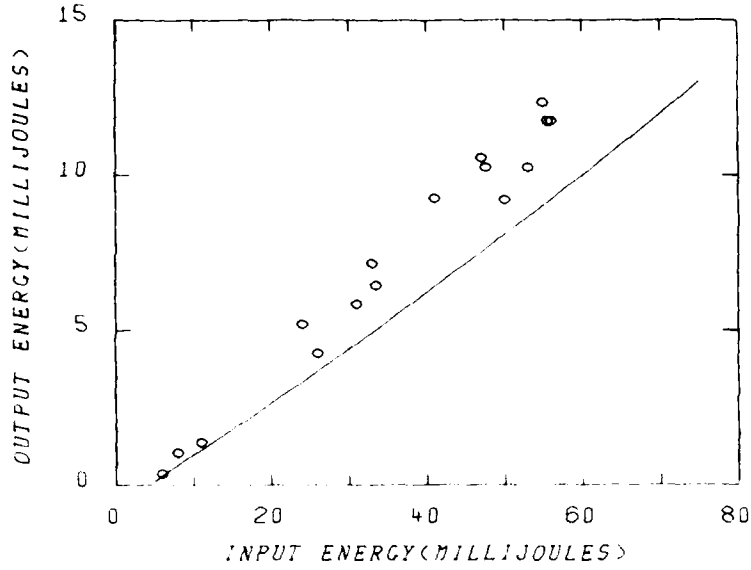

FIGURE 17 - Untuned P-T-P laser output energy as a function of Xe-Cl pumping energy

--o-- Uchino et al's experiment (Ref. 8)

——— theory

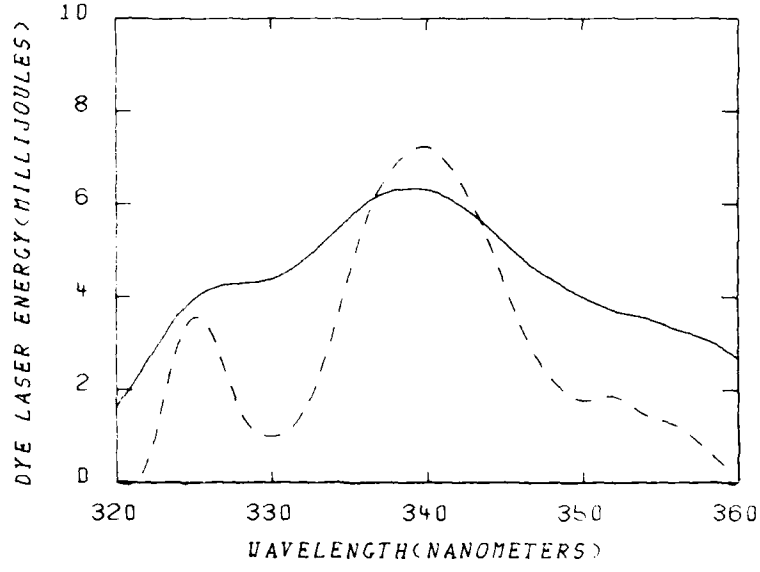

FIGURE 18 - Tunable P-T-P laser output efficiency as a function of wavelength. Xe-Cl laser pump.

------ Hollins' experimental results (Ref. 7)

——— theory

6.0 CONCLUSIONS AND RECOMMENDATIONS

Several conclusions can immediately be drawn from our results. The first of these is that Xe-Cl is a better pumping source for Para-Terphenyl than Kr-F, partly because a higher concentration of P-T-P is required to achieve a given penetration depth. This increases the gain density while leaving all the other losses unchanged. Another part of the improvement is due to the smaller energy difference between the pump laser and the Para-Terphenyl laser emission in the case of Xe-Cl.

The second improvement suggested by the theory is the use of deoxygenated solutions. In practice, some of the gain obtained could easily be offset by a substantial increase in the complexity of the equipment required to deoxygenate Para-Terphenyl, particularly in a circulating system for high repetition rate operation.

The third area for improvement is the solvent used. We have seen that in cyclohexane, pulse length and efficiency are strongly dependent on triplet-triplet absorption effects. If a solvent with a smaller shift toward the short wavelength could be found, such effects would become less important and it would be possible to operate with much longer pumping pulses (50-100 ns). This is a possible interpretation of recent results obtained for a Xe-Cl pump pulse of 50 ns duration using P-Dioxane as a solvent (Ref. 16).

The last and most important conclusion to be drawn from our model studies is that an oscillator-amplifier configuration should be used for maximum efficiency. The most advantageous feature of P-Terphenyl as a laser is its large tunable range. It is an ideal replacement for the low efficiency nitrogen laser.

The dispersive optical elements necessary for tuning (prisms, gratings, Fabry-Perot etalons, etc) all cause substantial losses in an oscillator cavity: gratings because of their inherent inefficiency, the other elements because they force us to lengthen the cavity, thereby increasing the diffraction losses. This situation can be remedied by using a small fraction of the total pump pulse energy to excite a tunable oscillator and the remaining pump energy to excite an amplifier in which the losses can easily be minimized. If a beam expander is used to couple the output of the oscillator into the amplifier, and if a smaller concentration of dye is used in the amplifier, so that the pump radiation penetration depth matches the beam expansion ratio, the diffraction losses become negligible. We can afford this large volume in an amplifier because we do not have to maintain as large a gain as in an oscillator. To efficiently extract the laser energy in an oscillator, saturation must be reached as fast as possible, therefore, the gain must be accordingly high for the pulse length is short. This constraint is considerably reduced in an amplifier so we can afford a large volume with a much smaller gain.

When one considers the possibility of high repetition rate operation, > 50 pps, an oscillator-amplifier becomes even more attractive. The dye cell windows of a laser can stand a few J/cm^2 of optical loading before damage occurs. In a P-T-P laser, in order to achieve high gains, the optimum penetration is approximately 1 mm or less. A square output beam shape means that the pulse energy of the P-T-P laser must be kept below 20 mJ, otherwise the dye cell will be damaged. Because of the larger penetration depth usable in an amplifier, this problem is alleviated and high energy pulses can be obtained at high repetition rate. The larger size of the dye amplifier also helps in terms of the flow problems encountered in a circulating high repetition rate system (Ref. 17).

7.0 EXPERIMENTAL IMPLEMENTATION AT DREV

Figures 19 and 20 are schematics of the experimental oscillator-amplifier built at DREV. The pump source was a Lumonics 262-2 excimer laser. Despite the fact that its expected efficiency is inferior to that of Xe-Cl, Kr-F was chosen because the 262-2 produces twice as much energy with Kr-F than with Xe-Cl. Furthermore, to reach a reasonable value of divergence and therefore line width, the pulse length had to exceed 15 ns and it is only 6 ns in Xe-Cl whereas it is about 20 ns in Kr-F.

In Fig. 20, the Kr-F beam, which is 20-mm wide and 8-mm high, is divided by a 50% beam splitter, M1. Part of the beam proceeds through the beam splitter and is focused on the surface of the dye cuvette, C1, by a cylindrical lens, L1. The cuvette has an optical path of 10 mm; it is tilted with respect to the vertical at an angle such that radiation reflected by grating G1 and the 50% reflectivity output coupler, M3, enter the dye at the Brewster angle. The cylindrical lens, L1, is inclined at an angle such that the pumping stripe is parallel to the optical axis of the laser through the dye cell (Ref. 7). Such an arrangement has the benefit of eliminating spurious Amplified Spontaneous Emission (A.S.E.) effects between the dye cell output windows while allowing the laser to be tuned by rotating G1 without having to realign the cavity at each wavelength. Lining up the cavity is also relatively straightforward when using an He-Ne beam. Other configurations were tested but they neither performed as well or combined all the advantages of this one.

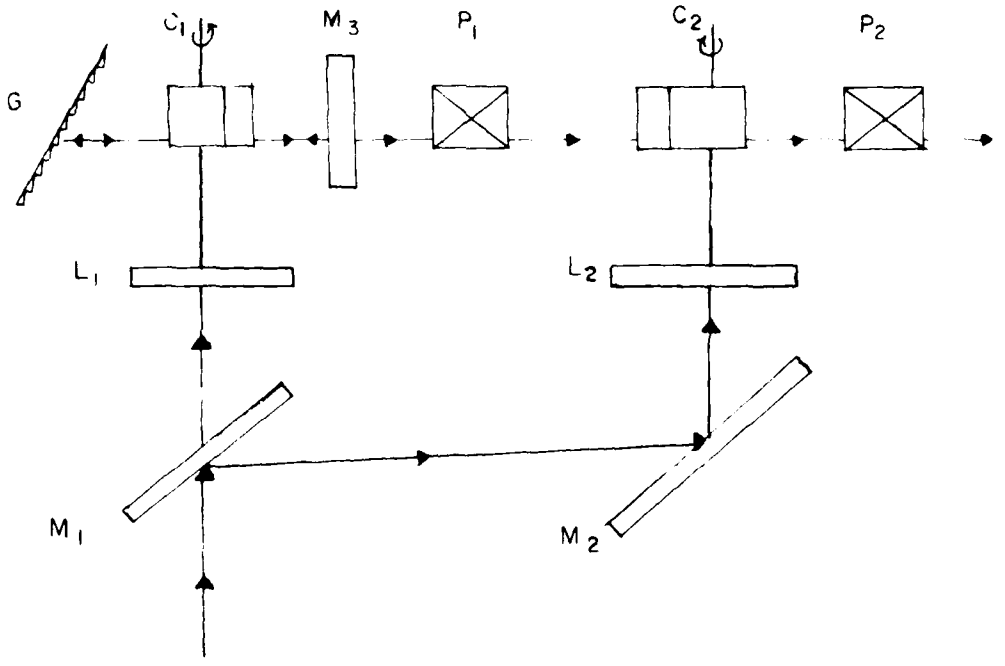

FIGURE 19 - Top view of an experimental oscillator-amplifier for P-T-P

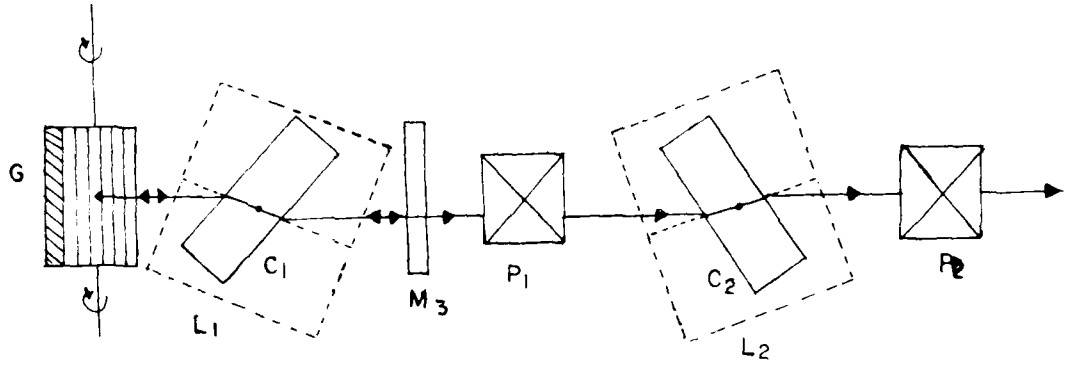

FIGURE 20 - Side view of an experimental oscillator-amplifier for P-T-P

The part of the beam reflected at M1 is sent to total reflector M2, and thence to cylindrical lens L2. There it is focused on the amplifier cell, C2, which is 20-mm wide and is also tilted at the Brewster angle. P1 is a Glan-Thompson polarizer used to reject any horizontally polarized component from the output beam of the oscillator and P2 is another Glan-Thompson prism in the output of the amplifier. By rotating P2, the output power of the oscillator-amplifier can be reduced in a controlled fashion without affecting such parameters as pulse length and output beam direction.

By setting mirror M2 back towards the pump laser source, an optical delay of 2 ns is introduced between mirrors M1 and M2 (this is not shown in Fig. 20). This delay was adjusted so that the dye oscillator could reach saturation before any pump energy arrived at the amplifier, C2. This ensures that the amplifier dye cell output windows do not serve as feedback elements and generate a significant amount of A.S.E. Grating G1 was 1200 lines/mm, blazed at 500 nm and was used in 2^{nd} order. The dye concentration was 3.3×10^{-4} Molar of P-T-P in "Instra-analyzed" cyclohexane from the J.T. Baker Chemical Co. 7 mJ of tuned radiation were extracted at 326.1 nm for a 65 mJ input energy to the amplifier. For both beams the energy was measured using the same ED 200 Joulemeter from Gen Tec. Some confidence can therefore be put on the efficiency measurement which yielded 10% at 326.1 nm. The 0.1 nm linewidth was measured through a spectroscope. The time dependence of the laser pulse was measured by a fast photodiode; it showed a 15 ns decay. Full optimization of the system has not yet been carried out since our primary purpose, i.e. to obtain a reliable source of radiation at 326.1 nm, was fulfilled.

Even without full optimization, the efficiency reported here at 326.1 nm is twice that obtained at this wavelength by previous investigators (Refs. 1, 4, 7). With a grating only and no beam expander of any kind, the linewidth is 3 times smaller than that reported by Zapka for a similar experiment (Ref. 1).

8.0 ACKNOWLEDGEMENTS

The author wishes to thank Dr. V.J. Beaulieu for several very helpful discussions during the course of this work.

9.0 REFERENCES

1. Zapka, W., Brackmann, U., Appl. Phys. 20, pp. 283-286 (1979)

2. Bücher, H., Chow, W. Appl. Phys. 13, p. 267 (1977)

3. Tomin, V.I., Alcock, A.J., Sarjeant, W.J., Leopold, K.E. Optics Commun. 26, pp. 396-400 (1978)

4. Tomin, V.I., Alcock, A.J., Sarjeant, W.J., Leopold, K.E. Optics Commun. 28, pp. 336-340 (1978)

5. Godard, B., de Witte, O. Optics Commun. 19, pp. 325-328 (1976)

6. McKee, T.J., James, D.J. Can. J. Phys. 57, pp. 1432-1436 (1979)

7. Hollins, R.C., D. Phil. Thesis Oxford University (1980)

8. Uchino, O., Mizunami, T., Maeda, M., Miyazoe, Y. Appl. Phys. 19 pp. 35-37 (1979)

9. Becker, R.S., "Theory and Interpretation of Fluorescence and Phosphorescence", Wiley. Interscience (1969)

10. Berlman, I.B., "Handbook of Fluorescence Spectra of Aromatic Molecules", Academic Press (1971)

11. Olmsted, J. III, J. Phys. Chem. 83, 20, pp. 2581-2584 (1979)

12. Mardelli, M., Olmsted, J., III, J. Photochem. 7, p. 377 (1977)

13. Heinzelmann, W., Labhart, H., Chem. Phys. Letters 4, 1, pp. 20-24 (1969)

14. Bensasson, R., Land, E.J., Trans. Faraday Soc. 67, pp. 1904-1915 (1971)

15. Pavlopoulos, T.J., Optics Commun., 24, 2, pp. 170-174 (1977)

16. Cassard, P., Taylor, R.S., Corkum, P.B., Alcock, A.J., SUBMITTED FOR PUBLICATION

17. Cassard, P., Corkum, P.B., Alcock, A.J., SUBMITTED TO APPLIED PHYSICS

18. Kellogg, R., Bennett, R., J. Chem. Phys. 41, p. 3042 (1964)

APPENDIX A

The possible reactions in an organic dye are shown in Fig. A-1 and listed in Table A-1.

Reaction (1) represents the absorption of pumping radiation by the ground singlet state of the dye. The cross section can be obtained by measuring the absorption of the dye solution along with its spectral profile [Ref. 9, pp. 84-86]. The Para-Terphenyl cross section is shown in Fig. 4.

Reaction (2) is the spontaneous emission for the singlet state which is generally referred to as fluorescence. The spectral integral of the cross section, given by reaction (1), is equal to the spectral integral of the cross section of reaction (2). Therefore, by simply measuring the spectral lineshape of fluorescence, one can determine the cross section of (2). The plot of this cross section is given in Fig. 3.

Reaction (3) is the radiationless transition from the first excited singlet to the first excited triplet. It is forbidden to first order; it only occurs because of spin-orbit coupling. The strength of this transition is very sensitive to the energy gap between the singlet and triplet states. In some dyes, part of the triplet state rovibrational energy band can coincide with the bottom of the singlet state one, giving rise to a significant transition probability. This is the case in Para-Terphenyl.

In reaction (4) the pump photons are absorbed and give rise to a transition from the first excited singlet to higher lying singlet states. For this reaction, the cross section can be established if one knows the behavior of the fluorescence energy as a function of the power density of the pump beam.

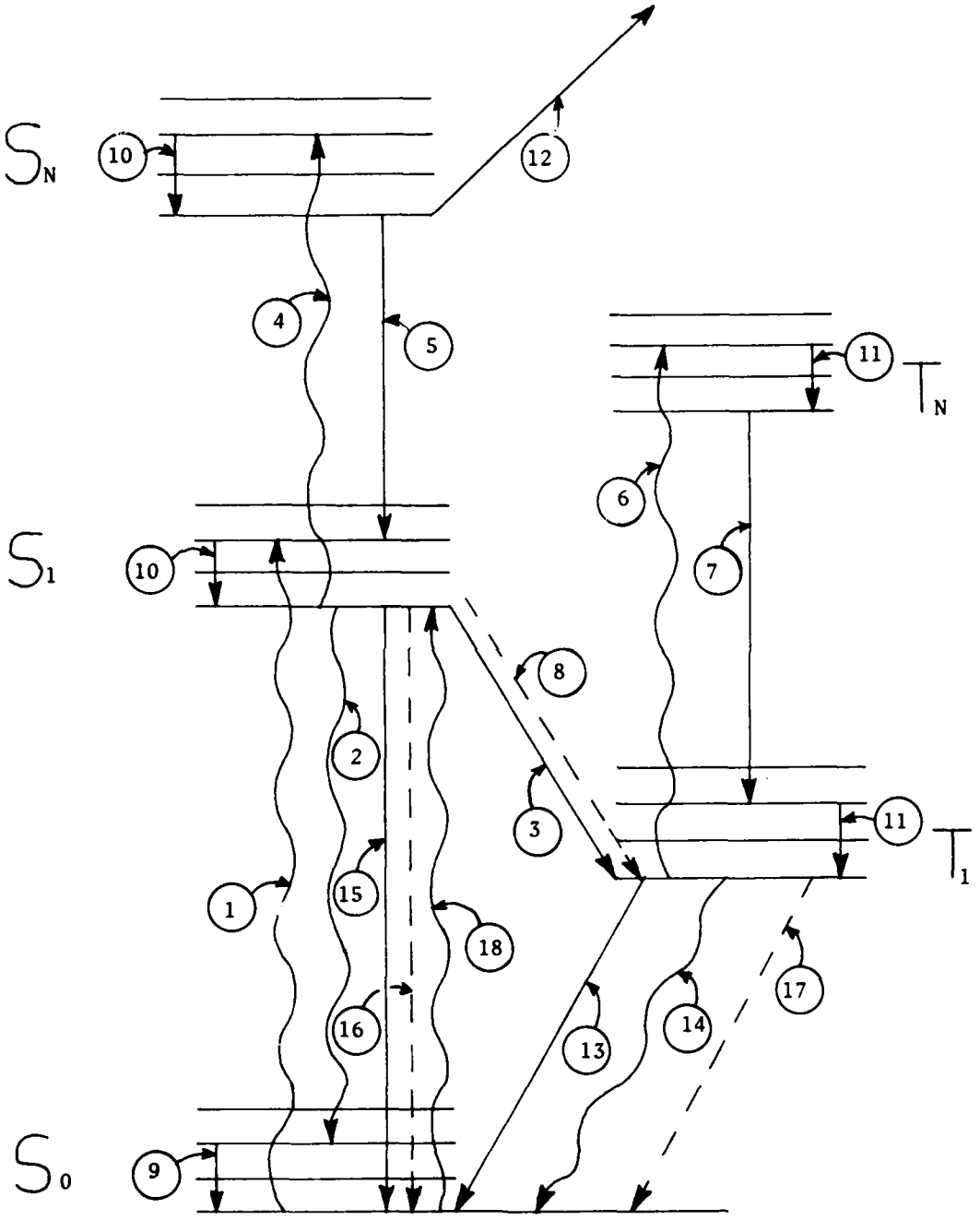

FIGURE A-1 - Energy diagram of Para-Terphenyl and reaction mechanisms in a dye

TABLE A-I

(1) $S_0 + h\nu_E \rightarrow S_1^*$

(2) $S_1 \rightarrow S_0^* + h\nu_f$

(3) $S_1 \rightarrow T_1$

(4) $S_1 \rightarrow S_n^*$

(5) $S_n \rightarrow S_1^*$

(6) $T_1 + h\nu_f \rightarrow T_n^*$

(7) $T_n \rightarrow T_1^*$

(8) $S_1 + O_2 \rightarrow T_1 + O_2$

(9) $S_0^* \rightarrow S_0$

(10) $S_1^* \rightarrow S_1$

$S_n^* \rightarrow S_n$

(11) $T_n^* \rightarrow T_n$

(12) $S_n \rightarrow$ Decomposition products

(13) $T_1 \rightarrow S_0$

(14) $T_1 \rightarrow S_0 + h\nu_p$

(15) $S_1 \rightarrow S_0$

(16) $S_1 + O_2 \rightarrow S_0 + O_2$

(17) $T_1 + O_2 \rightarrow S_0 + O_2$

(18) $S_0 + h\nu_f \rightarrow S_1$

Reaction (5), which describes a mechanism known as 'internal conversion', depends on the existence of curve crossings between the excited singlet states. If those crossings exist (they almost invariably do since the energy spectrum of most dyes is richly populated with states above the level of the first excited singlet), the downward transition probability approaches unity. Typical time scales for the relaxation of the high lying singlet states in a solution range from 10^{-11} to 10^{-14} seconds.

Reaction (6) accounts for the absorption of the fluorescence emitted in reaction (2) by a transition from the first excited triplet to higher triplet states. This reaction is the dominant quenching mechanism in laser emission from dyes on the long wavelength side of the emission spectrum.

Internal conversion which occurs within the manifold of excited triplet states is given by reaction (7). It arises from the mechanism described previously for reaction (5) and it generally takes place on the same time scale.

In general, dye solutions exposed to the atmosphere are nearly saturated with oxygen. Since O_2 is a highly para-magnetic substance, it acts as a strong perturber in spin-orbit transitions which rely on coupling between the magnetic fields generated by the electron spin and its orbital motion [Ref. 9, pp. 211 & 221]. This perturbation can substantially enhance the transition moment from singlet to triplet; it is accounted for in reaction (8).

Reactions (9), (10), and (11) describe the relaxation of the rovibrational energy bands of the different electronic states. In solution, at room temperature, this phenomenon is so fast (10^{-14} s) that all the manifold must be considered to be in a Boltzmann equilibrium.

Reaction (12) describes the photo-decomposition of the highly excited singlet states of the dye known to occur when certain dyes are subjected to intense ultraviolet radiation. It competes kinetically with reaction (5) as these are the only two-channels out of the excited singlet manifold. The long lifetime of laser action observed in Para-Terphenyl (over 500,000 shots to 1/e power) indicates that photo-decomposition is negligible or that it occurs at a rate which is much slower than that of internal conversion.

Reaction (13) represents radiationless decay from the T_1 to S_0 states. From the measurement of the phosphorescence quantum yield (Ref. 18) in Para-Terphenyl, which is 10% of the intersystem crossing quantum yield, we can establish that reaction (13) is 10 times faster than reaction (14) and is also negligible for our purposes.

Reaction (14) is the radiative transition from triplet to singlet; it is usually referred to as phosphorescence. This transition is forbidden and it occurs only because of spin-orbit coupling. In Para-Terphenyl, since the band gap between the T_1 and S_0 states is large, as in most other dyes, this spin-orbit contribution is small and the decay time is of the order of milliseconds. This is negligible over the 10^{-7} - 10^{-8} s time scales which are of interest to us.

Reaction (15) expresses the radiationless transition from the fluorescent state to S_0. As with reaction (5), a curve crossing is necessary, this time between the first excited singlet and the ground state. Para-Terphenyl has a very high quantum yield of fluorescence (0.88) thus if any reaction of the nature of (15) occurred, the minimum rate expected would be of the order of the spontaneous emission rate of Para-Terphenyl and it would give rise to a much smaller quantum yield [Ref. 9, pp. 121 & 134].

Reaction (16) represents the oxygen enhancement of the radiationless transition from S_1 to S_0. Since this transition is allowed, this effect can at best be of second order in perturbation theory. It is generally neglected compared to the effect of fluorescence (Ref. 9).

Reaction (17) is the analogue of reaction (8) but for the T_1 to S_0 transition. It is very important for many dyes as it allows the possibility of CW laser action by forming a channel whereby the population transferred to the triplet state by reactions (8) and (3) can be funnelled back to the ground state at a rate sufficient to allow laser action in the dye if a continuous pumping source is used. However, for this to occur several other conditions must be met. For instance, the triplet-triplet absorption must be sufficiently small over a large part of the fluorescence emission band. This is not the case in Para-Terphenyl and the rate of reaction (17) would have to be extremely large to be of any practical relevance. To be conservative in our estimates, we shall make the worst assumption and henceforth set the rate of reaction (17) to zero, because it can only help laser action.

Reaction (18) is only significant when one considers laser action. It represents the reabsorption of laser light by the ground state in the short wavelength limit of fluorescence (Fig. 5). It is given by the long wavelength limit of reaction (1) and was measured in Ref. 7. Because of (18), when one wishes to obtain lasing in the short wavelength side of 340 nm, it is necessary to insure that the entire length of the dye cuvette is excited by the pumping radiation.

CRDV R-4224/81 (NON CLASSIFIE)

Bureau - Recherche et Développement, MDN, Canada.
CRDV, C.P. 8800, Courcelette, Qué. G0A 1R0

"Un modèle du laser à colorant Para-Terphényl"
par G. Fournier

Nous avons conçu un modèle théorique de laser à colorant à base de Para-Terphényl pompé par un laser excimère et nous avons établi un nouveau groupe de coefficients pour les taux de réactions du Para-Terphényl. Le problème de l'émission spontanée dans le colorant a été solutionné analytiquement. Les solutions numériques des équations du laser sont assez conformes aux résultats des expériences relatées dans la littérature.

Le modèle que nous avons élaboré nous a permis d'atteindre une efficacité et une pureté spectrale encore inconnues. (NC)

CRDV R-4224/81 (NON CLASSIFIE)

Bureau - Recherche et Développement, MDN, Canada.
CRDV, C.P. 8800, Courcelette, Qué. G0A 1R0

"Un modèle du laser à colorant Para-Terphényl"
par G. Fournier

Nous avons conçu un modèle théorique de laser à colorant à base de Para-Terphényl pompé par un laser excimère et nous avons établi un nouveau groupe de coefficients pour les taux de réactions du Para-Terphényl. Le problème de l'émission spontanée dans le colorant a été solutionné analytiquement. Les solutions numériques des équations du laser sont assez conformes aux résultats des expériences relatées dans la littérature.

Le modèle que nous avons élaboré nous a permis d'atteindre une efficacité et une pureté spectrale encore inconnues. (NC)

CRDV R-4224/81 (NON CLASSIFIE)

Bureau - Recherche et Développement, MDN, Canada.
CRDV, C.P. 8800, Courcelette, Qué. G0A 1R0

"Un modèle du laser à colorant Para-Terphényl"
par G. Fournier

Nous avons conçu un modèle théorique de laser à colorant à base de Para-Terphényl pompé par un laser excimère et nous avons établi un nouveau groupe de coefficients pour les taux de réactions du Para-Terphényl. Le problème de l'émission spontanée dans le colorant a été solutionné analytiquement. Les solutions numériques des équations du laser sont assez conformes aux résultats des expériences relatées dans la littérature.

Le modèle que nous avons élaboré nous a permis d'atteindre une efficacité et une pureté spectrale encore inconnues. (NC)

CRDV R-4224/81 (NON CLASSIFIE)

Bureau - Recherche et Développement, MDN, Canada.
CRDV, C.P. 8800, Courcelette, Qué. G0A 1R0

"Un modèle du laser à colorant Para-Terphényl"
par G. Fournier

Nous avons conçu un modèle théorique de laser à colorant à base de Para-Terphényl pompé par un laser excimère et nous avons établi un nouveau groupe de coefficients pour les taux de réactions du Para-Terphényl. Le problème de l'émission spontanée dans le colorant a été solutionné analytiquement. Les solutions numériques des équations du laser sont assez conformes aux résultats des expériences relatées dans la littérature.

Le modèle que nous avons élaboré nous a permis d'atteindre une efficacité et une pureté spectrale encore inconnues. (NC)

DREV R-4224/81 (UNCLASSIFIED)

Research and Development Branch, DND, Canada.
DREV, P.O. Box 8800, Courcelette, Que. G0A 1R0

"A Model of the Para-Terphenyl Dye Laser"
by G. Fournier

A theoretical model for a Para-Terphenyl dye laser pumped by an excimer laser has been developed. A new set of reaction-rate coefficients for Para-Terphenyl has been established. The problem of spontaneous emission in a dye has been solved analytically. The numerical solutions of the laser equations agree closely with the experimental results reported in the literature.

Use of our model resulted in the achievement of higher efficiencies and narrower linewidths than those previously reported. (U)

DREV R-4224/81 (UNCLASSIFIED)

Research and Development Branch, DND, Canada.
DREV, P.O. Box 8800, Courcelette, Que. G0A 1R0

"A Model of the Para-Terphenyl Dye Laser"
by G. Fournier

A theoretical model for a Para-Terphenyl dye laser pumped by an excimer laser has been developed. A new set of reaction-rate coefficients for Para-Terphenyl has been established. The problem of spontaneous emission in a dye has been solved analytically. The numerical solutions of the laser equations agree closely with the experimental results reported in the literature.

Use of our model resulted in the achievement of higher efficiencies and narrower linewidths than those previously reported. (U)

DREV R-4224/81 (UNCLASSIFIED)

Research and Development Branch, DND, Canada.
DREV, P.O. Box 8800, Courcelette, Que. G0A 1R0

"A Model of the Para-Terphenyl Dye Laser"
by G. Fournier

A theoretical model for a Para-Terphenyl dye laser pumped by an excimer laser has been developed. A new set of reaction-rate coefficients for Para-Terphenyl has been established. The problem of spontaneous emission in a dye has been solved analytically. The numerical solutions of the laser equations agree closely with the experimental results reported in the literature.

Use of our model resulted in the achievement of higher efficiencies and narrower linewidths than those previously reported. (U)

DREV R-4224/81 (UNCLASSIFIED)

Research and Development Branch, DND, Canada.
DREV, P.O. Box 8800, Courcelette, Que. G0A 1R0

"A Model of the Para-Terphenyl Dye Laser"
by G. Fournier

A theoretical model for a Para-Terphenyl dye laser pumped by an excimer laser has been developed. A new set of reaction-rate coefficients for Para-Terphenyl has been established. The problem of spontaneous emission in a dye has been solved analytically. The numerical solutions of the laser equations agree closely with the experimental results reported in the literature.

Use of our model resulted in the achievement of higher efficiencies and narrower linewidths than those previously reported. (U)

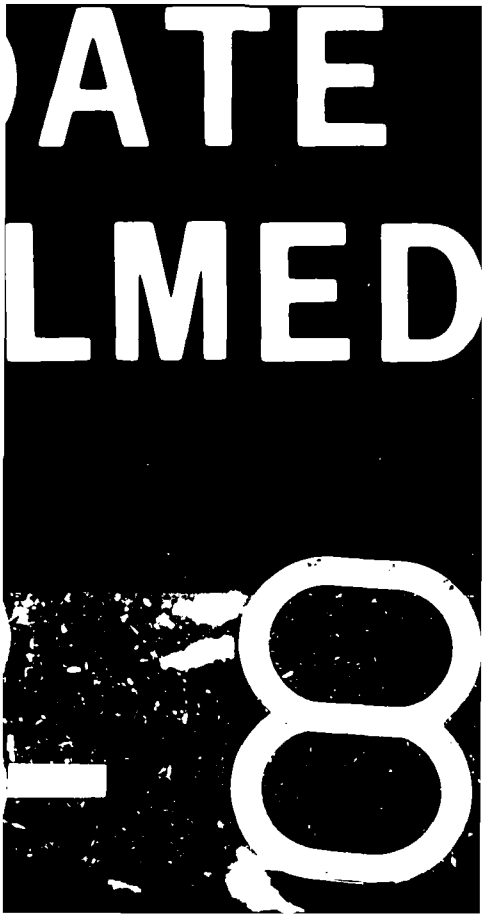
ATE
LMED
8